A dosimetric comparison of ^{169}Yb versus ^{192}Ir for HDR prostate brachytherapy

G. Lymperopoulou,[a] P. Papagiannis, and L. Sakelliou
Nuclear and Particle Physics Section, Physics Department, University of Athens, Panepistimioupolis, Ilisia, 157 71 Athens, Greece

N. Milickovic
Department of Medical Physics & Engineering, Strahlenklinik, Klinikum Offenbach, 63069 Offenbach, Germany

S. Giannouli
Pi-Medical Ltd., Research and Development Dept., Gennimata 2 Str., 115 24, Ampelokipoi, Athens, Greece

D. Baltas[b]
Department of Medical Physics & Engineering, Strahlenklinik, Klinikum Offenbach, 63069 Offenbach, Germany and Nuclear and Particle Physics Section, Physics Department, University of Athens, Panepistimioupolis, Ilisia, 157 71 Athens, Greece

(Received 14 July 2005; revised 6 September 2005; accepted for publication 29 September 2005; published 29 November 2005)

For the purpose of evaluating the use of ^{169}Yb for prostate High Dose Rate brachytherapy (HDR), a hypothetical ^{169}Yb source is assumed with the exact same design of the new microSelectron source replacing the ^{192}Ir active core by pure ^{169}Yb metal. Monte Carlo simulation is employed for the full dosimetric characterization of both sources and results are compared following the AAPM TG-43 dosimetric formalism. Monte Carlo calculated dosimetry results are incorporated in a commercially available treatment planning system (SWIFT^{TM}), which features an inverse treatment planning option based on a multiobjective dose optimization engine. The quality of prostate HDR brachytherapy using the real ^{192}Ir and hypothetical ^{169}Yb source is compared in a comprehensive analysis of different prostate implants in terms of the multiobjective dose optimization solutions as well as treatment quality indices such as Dose Volume Histograms (DVH) and the Conformal Index (COIN). Given that scattering overcompensates for absorption in intermediate photon energies and distances in the range of interest to prostate HDR brachytherapy, ^{169}Yb proves at least equivalent to ^{192}Ir irrespective of prostate volume. This has to be evaluated in view of the shielding requirements for the ^{169}Yb energies that are minimal relative to that for ^{192}Ir. © *2005 American Association of Physicists in Medicine*. [DOI: 10.1118/1.2126821]

I. INTRODUCTION

^{169}Yb was extensively studied in the past decade, mainly, as an alternative to ^{125}I and ^{103}Pd Low Dose Rate (LDR) seeds[1–3] and also to ^{192}Ir LDR and High Dose Rate (HDR) sources.[4,5] This culminated with the production of prototype ^{169}Yb sources that were used in a limited number of clinical trials.[6] While for LDR sources ^{125}I and ^{103}Pd were preferred over ^{169}Yb for radiation protection and radiobiological reasons,[1] the construction of ^{169}Yb HDR sources was obstructed by the low natural abundance of ^{168}Yb in the neutron activation reaction for the production of ^{169}Yb. However, on the grounds of its intermediate photon energy (93 keV emission probability weighted mean energy, 131 keV emission probability, and air kerma weighted effective energy) that could potentially provide increased dose homogeneity[4,7] with significantly reduced shielding requirements compared to higher energy radionuclides currently in use, ^{169}Yb appears to receive new focus lately[8–10] and the construction of HDR sources seems feasible.

One candidate application for the use of a new ^{169}Yb source is prostate HDR brachytherapy, which is currently performed in combination with external beam radiation therapy for dose escalation purposes[11–17] or monotherapy,[18–22] using ^{192}Ir sources (photon energy: 355 keV mean and 398 keV effective). Should ^{169}Yb provide an implant quality that is at least equivalent to that of ^{192}Ir, prostate HDR brachytherapy would greatly benefit from the reduction in shielding requirements for ^{169}Yb that would preclude the need for dedicated, heavily shielded suites and thus patient transfer from the urology or radiology department.

Seeking to test the above hypothesis, a comparison of dosimetric properties of the new microSelectron ^{192}Ir HDR source[23] versus a hypothetical ^{169}Yb HDR source of the same geometry with a pure ^{169}Yb metal active core is performed by means of a Monte Carlo simulation. Dosimetry results are then incorporated into a commercial Treatment Planning System (the SWIFT^{TM} TPS, Nucletron B.V. Veenendaal, The Netherlands) and a comprehensive analysis of different prostate treatment cases that are representative of the diversity met in clinical practice is performed for both sources using a multiobjective dose optimization-based, inverse treatment planning tool. Results are discussed in terms of the multiobjective dose optimization solutions as well as

TABLE I. The main implant characteristics for the prostate patient cases used for reporting results of this study.

Study case	PTV (cm^3)	Step Size (mm)	No. of catheters	No. of ASDPs[a]	ASDPs/cm^3
#1	36.23	2,5	16	205	5.66
#2	36.23	2,5	23	293	8.09
#3	76.68	2,5	20	331	4.32

[a]ASDPs: active source dwell positions.

treatment quality indices such as Dose Volume Histograms (DVH) and the Conformal Index (COIN).[24,25]

II. MATERIALS AND METHODS

A. Brachytherapy sources and Monte Carlo calculations

In order to perform a dosimetry comparison of the ^{192}Ir and ^{169}Yb radionuclides, the geometric configuration of the new microSelectron HDR source design was employed.[23] In this design, the cylindrical active source core is of 3.6 mm length and 0.65 mm diameter. The encapsulation is 0.9 mm in diameter, while the driving wire has a reduced diameter of 0.7 mm in order to increase the source flexibility. The encapsulation of the source is made of stainless steel (AISI 316L) with a percentage weight composition of 2% Mn, 1% Si, 17% Cr, 12% Ni, and 68% Fe, and a density of 8.02 g cm^{-3}. The wire is of the same composition with the encapsulation with its effective density equal to 4.81 g cm^{-3}, as measured by Daskalov *et al.* (1998).[23] The MCNPX code version 2. 4.0[26] was utilized to calculate the dosimetric properties of both the commercially available microSelectron HDR source design (with an ^{192}Ir metal core of 22.42 g cm^{-3} density, hereafter called the "^{192}Ir source") and a hypothetical source design with an ^{169}Yb active core (density of 6.73 g cm^{-3}, hereafter to be called "the ^{169}Yb source"). Although the dosimetry of the ^{192}Ir source is well known,[23] corresponding simulations were performed not only for benchmarking purposes but mainly to preclude potential systematic uncertainties that could obscure the comparison of results for the ^{192}Ir and ^{169}Yb sources. The initially emitted photon spectrum for the ^{192}Ir as well as for the ^{169}Yb source was taken from the NuDat database.[27] ^{169}Yb decays via electron capture to the stable ^{169}Tm with a half-life of 32.015 days.[27] Nonpenetrating photons of energy lower than 10 keV were not considered for both nuclides. Electron transport was not simulated in this study and the water collision kerma dose approximation was used.

Dose rate results in polar coordinates (according to the coordinate system recommended by the TG-43 formalism[28,29] with respect to the cylindrical source symmetry), were obtained using the CMESH:P pedep card, in simulations with the ^{192}Ir or ^{169}Yb source situated in the center of a spherical water phantom of 15 cm radius. The MCNPX mesh tally used overlays a cylindrical grid on the standard problem geometry and scores the energy deposition by photons per unit volume per initiated photon (MeV cm^{-3}photon^{-1}). The air kerma strength, S_K, of the ^{192}Ir and ^{169}Yb sources was calculated in separate runs, with each source in free space following the procedure described in Angelopoulos *et al.*[30] S_K results were used to express calculated dose rate values in water in units of cGy h^{-1} U^{-1} (1 U=1 μGy m^2 h^{-1}) and the resulting dose kernels were imported in the SWIFT^{TM} TPS assuming equal air kerma strength for the two sources.

15×10^6 initial photon histories were simulated in each run, resulting in statistical uncertainties of less than 1% at all points around the two sources, except for those lying close to the longitudinal axis of the sources where the statistical uncertainties are up to 3%.

B. Treatment plan evaluation

In order to compare the treatment quality in prostate HDR applications using the ^{192}Ir and ^{169}Yb sources, the inverse treatment planning feature of SWIFT^{TM} was utilized, which is based on a multiobjective anatomy-based dose optimization engine.[25,31–33]

Conformal anatomy-based dose optimization[25,31–33] considers the dose in the Planning Target Volume (PTV) as well as to the organs at risk (OARs) aiming to the complete coverage of the PTV with a dose at least equal to the prescription dose while simultaneously avoiding dose values above some predefined critical values for the organs at risk (critical structures). These critical values are OAR specific.

Optimization refers to the maximization or minimization of an objective function through determining (or approximating) the appropriate sets of values for its predetermined object parameters. In this work, the object parameters (input parameters) are the source dwell weights and dwell times. The output of the optimization is the objective value representing the quality of the solution. In a multicriteria optimization problem where many objectives are considered, the optimization produces a vector of objective values. In this study, four objective functions are considered; two related to the PTV (conformity and homogeneity) and two related to the organs at risk (urethra and rectum).

Concerning the PTV, the dose values are normalized using the average dose on the PTV surface, D_{ref}, which is set to be equal to the prescribed dose. The conformity objective, f_s, is defined as the normalized dose variance of the sampling points (dose points) uniformly distributed on the PTV surface. The uniformity objective, f_v, accounting for the avoidance of excessively high dose values inside the PTV, is the dose normalized variance of the dose distribution inside the PTV. These two objective functions are described by the following equations:

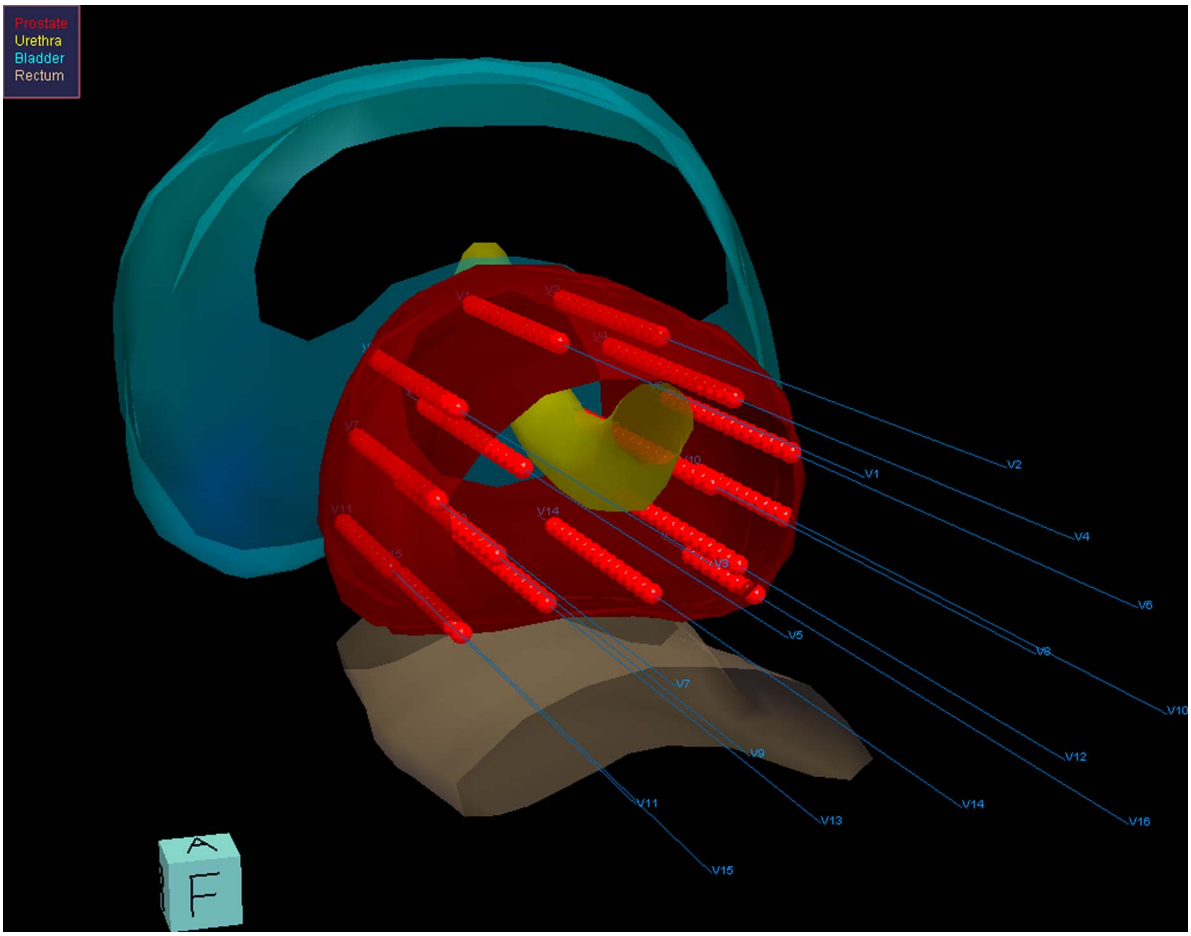

FIG. 1. A 3D graphical representation of the implant and the organs at risk (urethra, rectum, and bladder) for case #1. The catheters and the ASDPs available to the SWIFT Treatment Planning System are also depicted.

$$f_V = \frac{1}{N_V}\sum_{i=1}^{N_V}\frac{(d_i^V - m_V)^2}{m_V^2}, \tag{1}$$

$$f_S = \frac{1}{N_S}\sum_{i=1}^{N_S}\frac{(d_i^S - m_S)^2}{m_S^2}, \tag{2}$$

where d_i^V and d_i^S are the dose values of the ith sampling point on the PTV, surface and within the PTV, respectively, m_S and m_V are the corresponding average dose values, and N_S, N_V the corresponding numbers of sampling points.[25]

The objective functions of the organs at risk (urethra and rectum) are defined as

$$f_{\mathrm{OAR}} = \frac{1}{N_{\mathrm{OAR}}}\sum_{i=1}^{N_{\mathrm{OAR}}}\frac{\Theta(d_i^{\mathrm{OAR}} - D_{\mathrm{crit}}^{\mathrm{OAR}})(d_i^{\mathrm{OAR}} - D_{\mathrm{crit}}^{\mathrm{OAR}})^2}{(D_{\mathrm{crit}}^{\mathrm{OAR}})^2}, \tag{3}$$

where

$$\Theta(x) = \begin{cases} 1, & x < 0, \\ 0, & x > 0, \end{cases}$$

N_{OAR_i} is the number of sampling points in the OAR, and $D_{\mathrm{crit}}^{\mathrm{OAR}_i}$ is the corresponding critical dose as a fraction of the prescription dose or reference dose[25] that was chosen to be the average dose on the PTV surface.

It should be noted that each objective function should be as low as possible, in order to satisfy the goals of the optimization. In order to perform the optimization, the multiobjective problem is treated as a single objective, by combining the different objective functions $f_m(x)$ into a single objective function $f(x)$, using a weighted sum of all objectives:

$$f(\mathbf{x}) = \sum_{m=1}^{M} \mathrm{IF}_m f_m(\mathbf{x}); \tag{4}$$

$\mathbf{x}$ is the vector of source dwell weights or times and the weights IF_m are the importance factors and are considered as a measure of the significance of each objective in the optimization process, while in our study $M=4$. A representative convex part of the Pareto set[25] can be sampled by running a single objective optimization algorithm each time with a different vector of importance factors.

For each implant studied (see the following section), optimization was performed for 326 different combinations of importance factors using the "blind" optimization tool of SWIFT$^{\mathrm{TM}}$, representing a sample of the continuous space of all available not-dominated optimization solutions (pareto

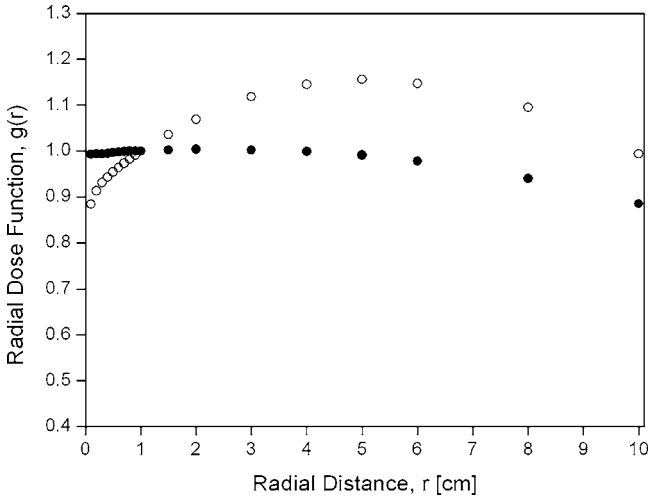

FIG. 2. Radial dose function values, $g(r)$, for the ^{192}Ir (●) and the ^{169}Yb (○) source.

space/front).[25] The resulting solutions were evaluated with respect to the influence of a relative objective weight to the brachytherapy treatment quality. In the optimization process, critical doses for the OARs were set to 150% of the prescribed dose for the urethra and 75% of the prescribed dose for the rectum (the bladder is not taken into account in the optimization process).

In this study, objective values were calculated using 10^3 sampling points uniformly distributed inside the PTV, 10^3 sampling points inside the urethra, rectum as well as bladder OAR, excluding points inside the catheters and an average number of five to ten sampling points per cm^2 on the PTV surface. A set of 2×10^4 sampling points were utilized for DVH calculations. Besides DVH, the COIN index[24,25] was also calculated for evaluating the treatment plans with the ^{192}Ir and ^{169}Yb sources, using 5×10^4 sampling points including points within the OARs as well as without considering the OARs. COIN is a measure of implant quality and dose specification in brachytherapy, and when not considering the OARs, it is defined for a specific dose value D as

$$\mathrm{COIN} = c_1 \cdot c_2, \tag{5}$$

where

$$c_1 = \frac{\mathrm{PTV}_D}{\mathrm{PTV}} \quad \text{and} \quad c_2 = \frac{\mathrm{PTV}_D}{V_D}.$$

The factor c_1 is the fraction of PTV (PTV_D) with dose values of at least D and is a measure of how accurately the PTV is covered by D. The factor c_2 is the fraction of the calculated (body) volume with dose values of at least $D(V_D)$ that is covered by the PTVand provides moreover a measure of how much normal tissue outside PTV is covered by D.

When the OARs are considered, COIN is modified by using a third factor c_3 according to

$$\mathrm{COIN} = c_1 \cdot c_2 \cdot c_3, \tag{6}$$

where

$$c_3 = \prod_{i=1}^{N_{\mathrm{OAR}}} \left(1 - \frac{V^i_{\mathrm{OAR}}(D > D^i_{\mathrm{crit}})}{V^i_{\mathrm{OAR}}}\right),$$

V^i_{OAR} is the volume of the ith OAR, and $V^i_{\mathrm{OAR}}(D>D^i_{\mathrm{crit}})$ is the volume of the ith OAR that receives a dose that exceeds the critical dose D^i_{crit}. It should be noted that although the dose delivered to the bladder is not a parameter of the optimization procedure, it is taken into account along with the urethra and the rectum in the COIN calculation ($N_{\mathrm{OAR}}=3$). In the following analysis, the maximum observed COIN value of each 3D dose distribution is considered.

C. Clinical cases studied

Four prostate cancer patients of 26.16, 36.23, 55.01, and 76.68 cm^3 PTV volume were used as the basis of this study in an effort to account for the diversity met in clinical prostate HDR brachytherapy boost and monotherapy applications. For each patient, two different numbers of catheters and consequently two different numbers of active source dwell positions (ASDPs) were evaluated; one typically used for HDR treatments, and one with the maximum number of implantable catheters in order to lift any bias of the inter comparison between the ^{192}Ir and ^{169}Yb sources from catheter placement. Hence, a total of eight different cases were studied.

The three selected cases summarized in Table I, are used in the following as the basis for reporting results of this study and the remaining five are discussed where appropriate. In Table I case #1 (which is also graphically presented in Fig. 1) and case #2 refer to an implant volume of 36 cm^3 which is typically within the range of the optimal PTV extent for monotherapy treatment while case #3 corresponds to the extreme case of a 77 cm^3 implant volume that lies on the upper limit for boost therapy. Case #2 differs from case #1 only in that it involves a greater number of catheters and thus an increased number of ASDPs are available to the optimization algorithm of the TPS, having a density of 8.09 ASPDs per cm^3, compared to 5.66 ASPDs per cm^3 of case #1.

III. RESULTS AND DISCUSSION

A. Comparison of dosimetric characteristics

The air kerma strength per unit contained activity for the ^{192}Ir source was found equal to $\left(\frac{S_K}{A}\right)_{^{192}\mathrm{Ir}}=0.098$ U MBq^{-1}, which is in excellent agreement (0.5%) with the corresponding result published by Borg and Rogers.[35] The corresponding result for the ^{169}Yb source was $\left(\frac{S_K}{A}\right)_{^{169}Yb}=0.030$ U MBq^{-1} which is about 70% lower than that for the ^{192}Ir source. Simulations for bare point sources yielded a corresponding air kerma strength per contained activity difference of 60% (0.109 U MBq^{-1} for ^{192}Ir and 0.043 U MBq^{-1} for ^{169}Yb).

The dose rate constant, Λ, of the ^{192}Ir source was found equal to $\Lambda_{^{192}\mathrm{Ir}}=(1.106\pm0.3\%)$ cGy h^{-1} U^{-1} in excellent agreement (0.2%) with that reported by Daskalov *et al.* (1998).[23] The corresponding result for the ^{169}Yb source was

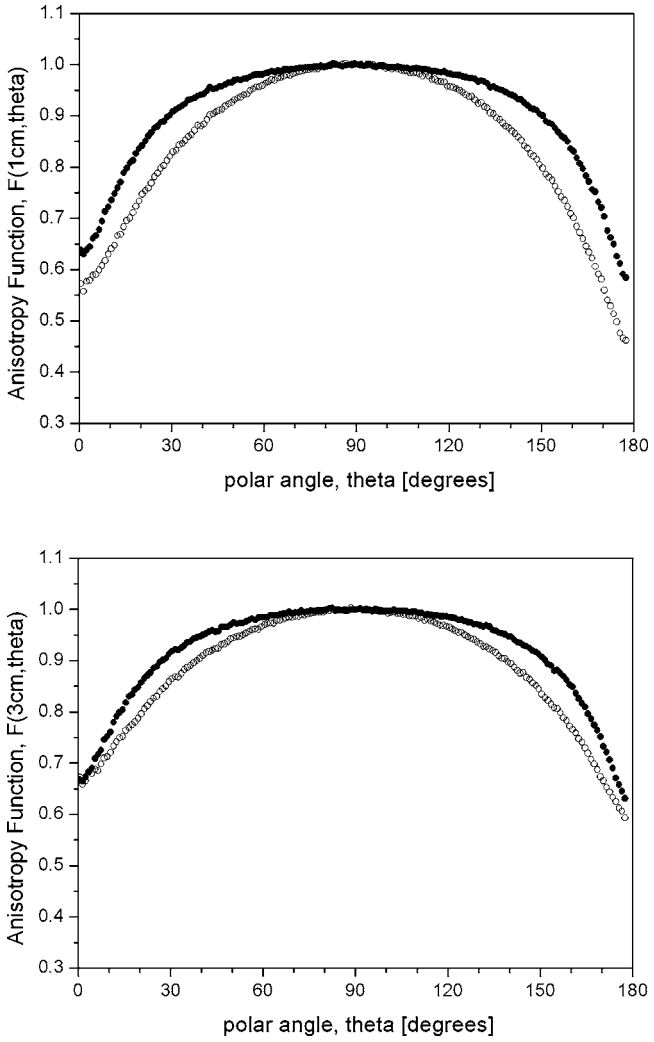

FIG. 3. Anisotropy function values plotted against polar angle for the ^{192}Ir (●) and the ^{169}Yb (○) source, at the radial distances of 1 and 3 cm.

$\Lambda_{^{169}\mathrm{Yb}}=(1.147\pm0.3\%)$ cGy h^{-1} U^{-1} which is 3.7% higher than that for ^{192}Ir. Separate test MC simulations showed that the latter percentage difference cannot be significantly enhanced by optimizing the ^{169}Yb source design in terms of active core dimensions and encapsulation material/thickness.

The above results imply that in order to achieve the same air kerma strength with a 370 GBq ^{192}Ir HDR source, a contained activity of approximately 1166 GBq is required for the ^{169}Yb source. This corresponds to a specific activity of 146 GBq mg^{-1} given the ytterbium mass in the core of the hypothetical source design considered herein (8.01 mg calculated by the active core volume of 1.19 mm^3 and the ytterbium metal density of 6.73 g cm^{-3}). Although other methods have been evaluated,[9] ^{169}Yb is commonly produced by the neutron activation of naturally occurring ^{168}Yb, which has an abundance of 0.13%. Given that the theoretical, maximum achievable specific activity for 100% purity in ^{168}Yb is about 893 GBq mg^{-1}, the required purity of ^{168}Yb is at least 16%. In view of the currently achievable ^{168}Yb enrichment of up to 85% using the cost efficient Calutron method, the production of ^{169}Yb HDR sources is technically feasible. This suggests that the only problem to be technically and economically evaluated with regard to a new ^{169}Yb HDR afterloader would be the frequent replacement of the source due to the lower half-life of ^{169}Yb relative to ^{192}Ir.

The radial dose function, $g(r)$, of the ^{192}Ir and ^{169}Yb sources, calculated by MC dose rates using the line source approximated source geometry factor, are plotted versus radial distance, r, in Fig. 2. This figure depicts the familiar interaction properties of intermediate photon energy emitters where multiple Compton scattering results to the gradual buildup of a significant scatter dose component with the distance from the source that overcompensates for absorption and leads to a maximum $g(r)$ value of 1.15 at about 5 cm. In comparison, for the higher photon energies of ^{192}Ir scatter just compensates for absorption, resulting in a slow-varying $g(r)$ function with values close to unity and a transverse axis dose distribution that follows the geometry factor falloff with distance. Thus, the increased $g(r)$ and Λ partly make up for the increased contained activity necessary for the ^{169}Yb source to achieve HDR treatments in comparable treatment times to those of ^{192}Ir.

In Fig. 3, anisotropy function, $F(r,\theta)$, values calculated by MC dose rates using the line source approximated source geometry factor are plotted for the two sources versus polar angle θ at selected radial distances of 1 and 3 cm. In this figure it can be seen that the dose distribution anisotropy is more pronounced for the ^{169}Yb source as expected by the lower emitted photon energies, which lead to increased self-absorption and attenuation in the source structure.

B. Multiobjective dose optimization results

1. Objective functions

The solutions of the multiobjective dose optimization are presented in Fig. 4 for case #1, which is considered as the reference with respect to PTV volume, in the form of two-dimensional plots of the correlation between the objective results, for the ^{192}Ir and ^{169}Yb sources.

Figure 4 demonstrates the 6 possible two-dimensional projections of the 326 non dominated solutions obtained with the "blind" multiobjective optimization of SWIFT^{TM}, which is a representative discrete sampling of the non dominated solution space (i.e., the four-dimensional pareto front, due to the four objectives considered).[25,31–34] It should be noted that the lower the value of the objective function (see Eq. (1)–(3)), the better the quality of the dose distribution regarding this objective.

In addition, in Fig. 4 regions of extreme solutions (corresponding to very low or zero objective IF) are delineated to facilitate an overview of the correlation between the different objectives. This correlation can be seen to be of the same form for both the ^{192}Ir and ^{169}Yb sources. In a qualitative comparison of dose optimization solutions for the two sources, the ^{169}Yb source can be seen to yield lower conformity objective values (higher conformity) relative to the ^{192}Ir source while maintaining lower homogeneity [Fig. 4(a)] and urethra [Fig. 4(b)] objective values, which corresponds to better homogeneity inside the PTV and better sparing of the

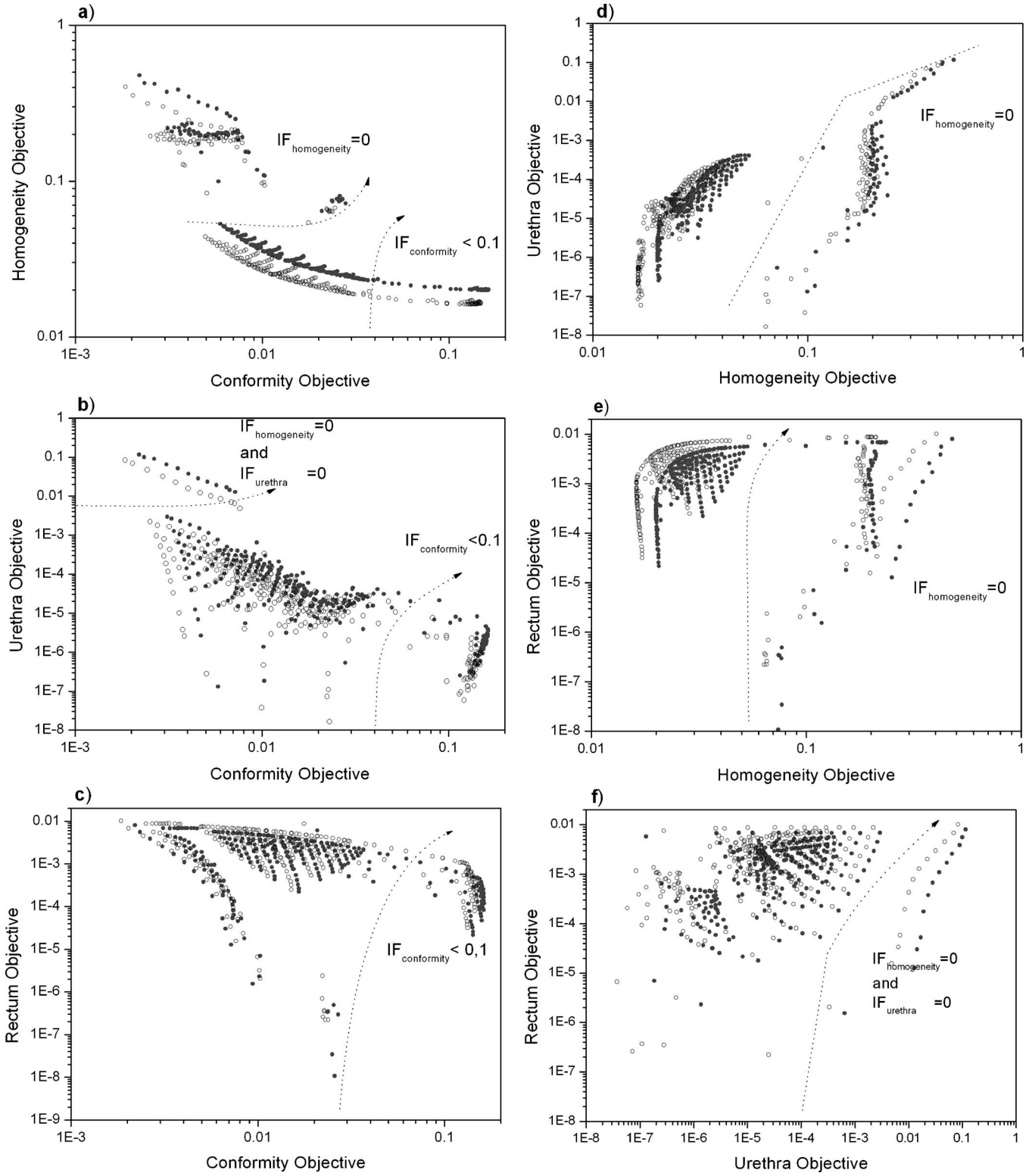

FIG. 4. Two-dimensional projections of the nondominated solutions obtained by the optimization for the ^{192}Ir (●) and the ^{169}Yb (○) source in study case #1. It should be noted that the lower the value of the objective function, the better the quality of the dose distribution regarding this objective.

urethra. Figure 4(c), however, suggests that ^{169}Yb solutions with lower conformity objective values present increased rectum objective values relative to ^{192}Ir. In terms of homogeneity, ^{169}Yb achieves lower objective values (better homogeneity) relative to ^{192}Ir while maintaining lower conformity [Fig. 4(a)] and urethra [Fig. 4(d)] objective values. Reduced homogeneity objective values for the dose optimization solutions with the ^{169}Yb source, however, come at the expense of increased rectum objective values relative to the ^{192}Ir source [Fig. 4(e)]. Figure 4(f) presents objective values re-

TABLE II. Characteristic DVH parameters of ^{192}Ir vs ^{169}Yb source for the PTV in the three patient cases presented herein. SD: standard deviation.

		D_{min}	D_{max}	D_{90}	V_{100}	V_{150}	V_{200}
				Case #1			
^{192}Ir	mean±1SD	71.5±5.4	817.3±431.5	103.7±5.4	92.1±4.4	29.2±13.6	7.9±5.8
	min, max	60.9, 87.1	303.8, 2237.8	94.3, 113.4	82.7, 98.9	10.5, 58.5	2.8, 32.4
^{169}Yb	mean±1SD	73.7±5.2	731.2±386.2	104.0±4.9	92.6±4.1	24.9±12.6	6.0±4.6
	min, max	63.06, 88.1	284.5, 2219.7	95.0, 112.8	83.0, 99.0	8.6, 55.7	2.2, 27.4
				Case #2			
^{192}Ir	mean±1SD	71.6±7.3	797.0±417.9	105.6±4.8	93.7±3.3	28.3±15.2	7.6±7.2
	min, max	59.9, 86.5	291.5, 2116.6	97.5, 113.6	87.4, 99.1	9.6, 58.9	2.3, 31.1
^{169}Yb	mean±1SD	73.4±6.7	722.9±368.9	105.6±4.4	94.0±3.1	23.5±14	5.6±5.6
	min, max	61.9, 87.2	264.2, 1902.7	94.8, 113.0	86.1, 99.2	7.4, 55.7	1.7, 27.0
				Case #3			
^{192}Ir	mean±1SD	69.1±7.3	938.6±260.2	100.9±6.1	90.1±5.8	33.0±15.0	9.8±7.0
	min, max	56.9, 82.8	329.9, 1938.0	88.8, 108.2	77.2, 97.0	8.9, 56.0	2.9, 32.0
^{169}Yb	mean±1SD	71.0±6.8	830.2±239.6	101.0±5.3	90.4±5.3	27.4±14.1	7.3±5.5
	min, max	59.9, 83.7	291.3, 1694.7	90.5, 107.5	78.9, 97.0	7.3, 52.8	2.3, 26.6

TABLE III. Characteristic DVH parameters of ^{192}Ir vs ^{169}Yb source for the urethra and rectum OAR, in the three cases present herein. SD: standard deviation.

		Urethra			Rectum		
		D_{10}(%)	D_{max}(%)	V_{crit}(%)	D_{10}(%)	D_{max}(%)	V_{crit}(%)
				Case #1			
^{192}Ir	mean±1SD	122.3±20.0	167.0±24.5	2.7±10.1	66.3±2.7	85.6±5.1	3.4±1.9
	min, max	101.2, 231.7	134.0, 305.5	0.0, 54.9	60.6, 73.9	73.1, 94.0	0.1, 9.1
^{169}Yb	mean±1SD	122.8±17.1	163.5±20.5	2.1±8.3	68.8±2.9	86.4±5.6	4.6±2.4
	min, max	103.0, 219.8	133.3, 290.9	0.0, 54.4	62.8, 76.5	74.6, 96.0	0.2, 11.5
				Case #2			
^{192}Ir	mean±1SD	125.4±21.6	147.4±33.5	0.9±4.9	65.5±2.5	84.0±5.0	3.0±1.8
	min, max	103.2, 223.5	112.3, 292.1	0.0, 45.0	61.8, 73.7	72.5, 97.0	0.0, 9.6
^{169}Yb	mean±1SD	125.1±19.2	145.0±31.0	0.6±3.6	67.9±3.3	85.1±5.4	4.1±2.6
	min, max	105.6, 210.3	111.5, 269.0	0.0, 42.7	58.9, 76.7	70.7, 99.0	0, 11.9
				Case #3			
^{192}Ir	mean±1SD	130.6±19.0	148.5±32.0	3.3±11.8	66.8±3.9	88.1±3.0	3.2±1.9
	min, max	102.6, 220.1	113.3, 295.9	0.0, 67.5	58.9, 73.8	72.7, 106.1	0.0, 8.7
^{169}Yb	mean±1SD	128.9±16.3	144.7±28.3	2.5±9.5	69.2±3.6	88.0±7.2	4.5±2.6
	min, max	106.0, 204.7	113.6, 263.4	0.0, 66.9	62.3, 75.8	73.7, 105.1	0.1, 11

TABLE IV. Minimum, maximum, and average conformal index (COIN) values and corresponding standard deviations calculated (i) including the OARs [Eq. (6)] and (ii) without including the OARs [Eq. (5)] for the ^{192}Ir and the ^{192}Yb source. SD: standard deviation.

		Case #1		Case #2		Case #3	
		COIN OARs included	COIN OARs not included	COIN OARs included	COIN OARs not included	COIN OARs included	COIN OARs not included
^{192}Ir	mean±1SD*	0.851±0.087	0.918±0.027	0.855±0.047	0.935±0.020	0.815±0.099	0.888±0.025
	min, max	0.390, 0.897	0.865, 0.977	0.460, 0.925	0.896, 0.978	0.275, 0.927	0.844, 0.959
^{169}Yb	mean±1SD	0.842±0.091	0.920±0.027	0.883±0.035	0.935±0.022	0.809±0.081	0.885±0.023
	min, max	0.382, 0.890	0.851, 0.979	0.489, 0.913	0.864, 0.978	0.273, 0.912	0.840, 0.959

sults for the two OARs and it can be seen that, on average, ^{169}Yb yields lower urethra and higher rectum objective values relative to ^{192}Ir.

The above qualitative analysis suggests that the ^{169}Yb source better facilitates PTV conformity achieving improved urethra sparing while maintaining a more homogenous distribution inside the PTV relative to ^{192}Ir. The ^{169}Yb source, however, could lead to increased rectum dosage if this organ at risk is not carefully considered in the dose optimization procedure.

The rest of the studied prostate cases (see Sec. II C) yielded similar results for varying the prostate volume. A comparison of treatment plans for the same patient, but with a different number of ASDPs, showed that the increase of, ASDP number yields corresponding results for the comparison of the ^{169}Yb and ^{192}Ir sources leading, however, to less extreme solutions due to the smaller variability of the homogeneity and urethra objective values (for example, concerning case #2 the urethra objective equals to zero for every solution, which takes into account the homogeneity objective). A corresponding, yet less pronounced, effect was observed with the increase of ASDPs for the homogeneity objective while the rectum objective was not affected significantly.

2. Dose volume histograms and dosimetric indices

The multiobjective dose optimization solutions for the ^{192}Ir and ^{169}Yb sources are discussed in this section in the form of DVH parameters and COIN values that constitute treatment planning quality indices. DVH parameters for the PTV and the OARs are summarized in Tables II and III, respectively. Results in Table II show some common characteristics for all three cases. PTV $D_{\max}$ is, on average, lower for ^{169}Yb relative to ^{192}Ir implying better homogeneity inside the prostate. This is also supported by the slightly lower average values of $D_{\min}$ for ^{169}Yb. Moreover, V_{150} and V_{200} are 15%–20% greater for ^{192}Ir relative to ^{169}Yb. Results in Table III show that urethra D_{10} is, on average, comparable for both ^{169}Yb and ^{192}Ir, with the latter presenting greater standard deviations. However, maximum urethra dose is on the average slightly lower for ^{169}Yb and V_{critical} (the percentage of OAR volume receiving more than the set dose limit of 150% of the prescribed dose) is, on average, better for ^{169}Yb. On the contrary, for the rectum OAR ^{192}Ir yields better results with lower average values and smaller standard deviations. DVH calculations for the bladder, which constitutes an OAR that was not taken into account in the dose optimization showed no significant differences between ^{192}Ir and ^{169}Yb in all cases. As indicated by results in the previous section, overall ^{169}Yb yields better dose homogeneity inside the PTV, which generally corresponds to lower dosage of the urethra. On the other hand, the greater values of the rectum objective for ^{169}Yb compared to ^{192}Ir (see Fig. 4) are reflected in the less effective sparing of this organ when ^{192}Yb is used. However, it should be noted that the extremes for rectum are observed when this organ is not included in the optimization process ($IF_{\text{rectum}}=0$).

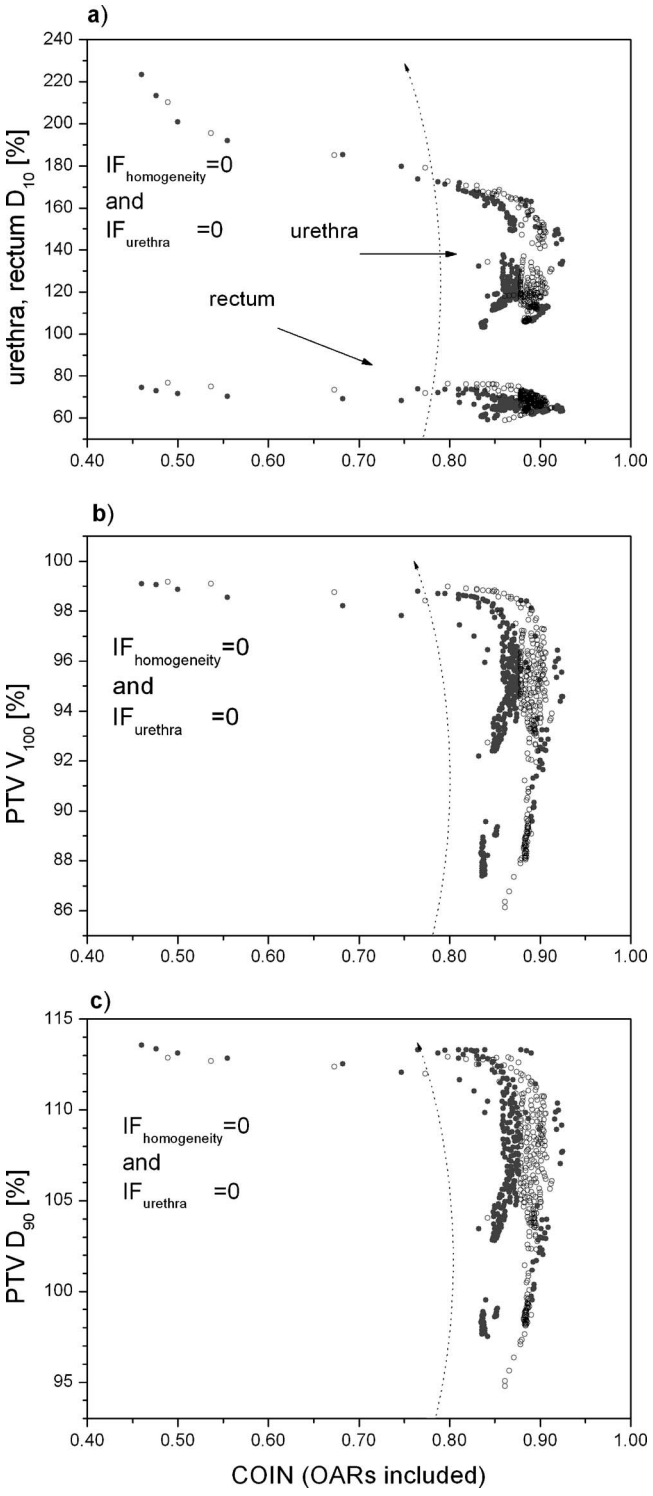

FIG. 5. Conformal Index (COIN) (Refs. 24 and 25) results calculated with considering the OARs [Eq. (6)], plotted versus urethra/rectum D_{10} (a), PTV V_{100} (b) and PTV D_{90} (c) for the ^{192}Ir (●) and the ^{169}Yb (○) source.

Table IV summarizes COIN results for the dose optimization solutions in the three treatment cases used herein as the basis for reporting results. Tabulated values show that not considering the OARs yields, as expected, greater average COIN values that are comparable for both the ^{192}Ir and ^{169}Yb sources. When the OARs are also considered, a good agree-

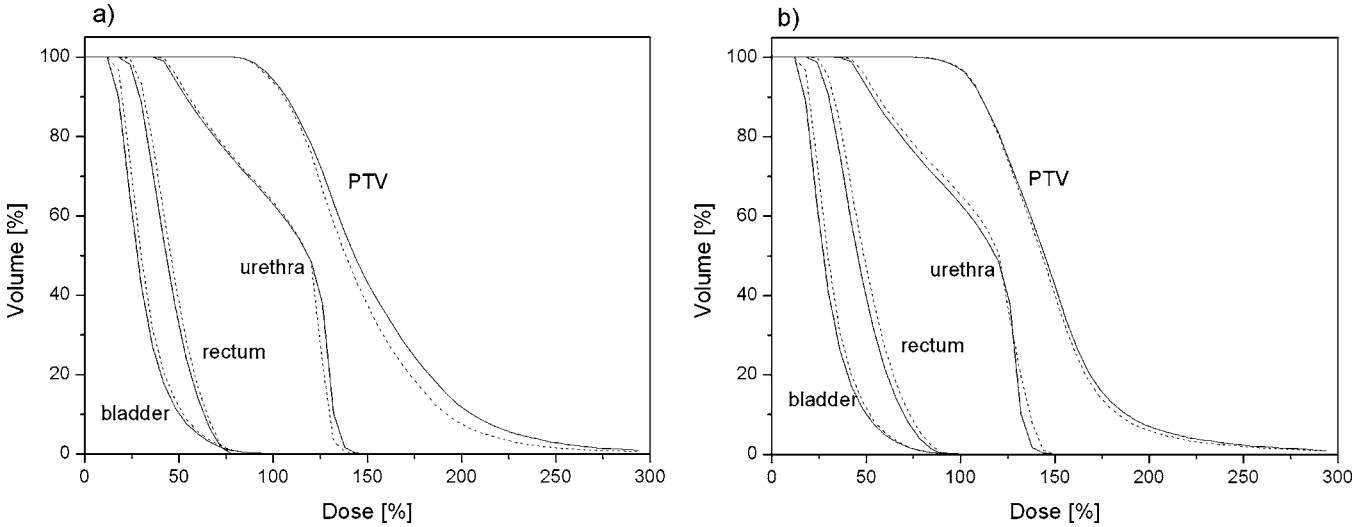

FIG. 6. Cumulative DVH for case #2 for the ^{192}Ir (solid lines) and the ^{169}Yb (dashed lines) sources for the selected inverse planning solution (a) including OARs and (b) without considering the OARs in the COIN calculation.

ment between COIN results for ^{192}Ir and ^{169}Yb is observed for case #2, which involves an increased number of available ASDPs while for the remaining two cases the ^{192}Ir source achieves greater COIN results.

COIN values of the dose optimization solutions for case #2, calculated by taking the urethra, rectum, and bladder OAR into account, are also plotted in Fig. 5 versus the selected parameters of OAR D_{10} and PTV V_{100} and D_{90}. Regarding COIN results, taking into account the OARs [Figs. 5(a)–5(c)] there appears to be a limited number of solutions corresponding to very low COIN values for both nuclides. These extremes are optimization solutions where neither uniformity nor urethra are taken into account (i.e., IF=0) leading to increased dosage of normal tissue outside the prostate. Otherwise, Figs. 5(a)–5(c) suggest that for comparable COIN values the ^{169}Yb source achieves comparable urethra D_{10} and PTV D_{90} values, greater rectum D_{10} and PTV V_{100} values. The same results are drawn from the comparison of COIN values for the ^{169}Yb and ^{192}Ir sources calculated without taking the OARs into account. It is worth noting, however, that ^{169}Yb COIN results calculated without taking the OARs into account extend to lower values compared to ^{192}Ir. Moreover, COIN without taking the OARs into account should be used with caution since maximum COIN values could lead to increased urethra dosage, especially for zero homogeneity IF.

3. Comparison of ^{192}Ir and ^{169}Yb for selected solutions

For the purpose of simplifying the comparison of prostate HDR treatment quality using the ^{192}Ir and ^{169}Yb sources, an inverse dose optimization solution was selected for each studied case (hereafter to be called the selected plan). This selection was based on maximum COIN with and without

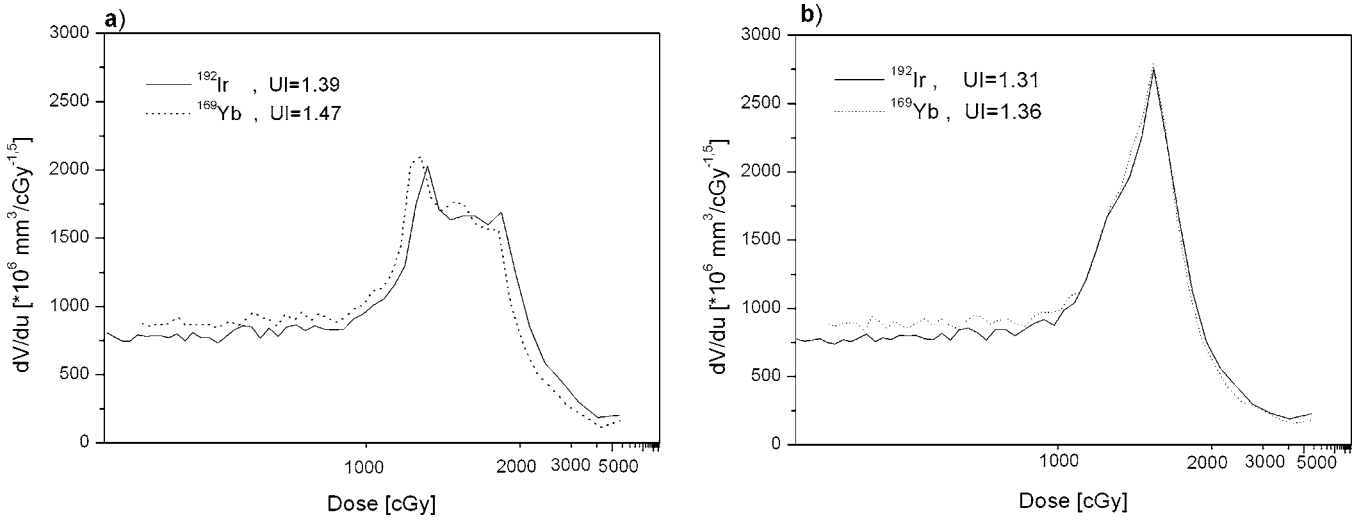

FIG. 7. Natural DVH[36,37] for case #2 for the ^{192}Ir and the ^{169}Yb sources for the selected inverse planning solution (a) including OARs and (b) without considering the OARs in the COIN calculation. Corresponding uniformity indices (UI) are also presented.

taking the OARs into account, in combination with the following additional criteria:[21] PTV $V_{100} \geqslant 90\%$, PTV $D_{90} \geqslant 100\%$, PTV $V_{200} < 10\%$ for cases #1, #2 and PTV $V_{200} < 20\%$ for case #3, $D_{10,\text{uret}} \leqslant 175\%$, $D_{\max,\text{uret}} \leqslant 200\%$, $D_{10,\text{rect}} \leqslant 75\%$ and $D_{\max,\text{rect}} \leqslant 90\%$.

The cumulative and natural DVH were calculated for the two selected plans for each studied case and representative results are shown for case #2 in Figs. 6 and 7, respectively. Cumulative DVH results of Fig. 6 are comparable for the two sources, indicating that the ^{169}Yb source achieves slightly improved uniformity with lower doses within the PTV and slightly worse OAR sparing, except for the urethra, when the OARs are included in COIN calculation [Fig. 6(a)]. Natural DVH[36,37] results presented in Fig. 7 yield better Uniformity Index values for the ^{169}Yb source for both optimum plans (with and without including the OARs in COIN calculation). This was also observed in results for cases #1 and #3.

For the selected plans, the Integral Dose delivered to the PTV as well as the patient body was calculated using the differential DVH. Results indicate that irrespective of the source used for the treatment, the same amount of energy is absorbed by the implant and the surrounding tissue. Moreover, the number of the active source dwell positions actually used by the treatment planning system (dwell time >0) for the optimum plan presents no significant difference for the ^{169}Yb and ^{192}Ir sources. Finally, total treatment times per unit source strength were found almost identical for the two sources, underlying the equivalence of the prostate treatment with the ^{192}Ir and the ^{169}Yb source.

IV. CONCLUSIONS

The dosimetric characteristics of a hypothetical ^{169}Yb source, with the exact same design of the new microSelectron source, replacing the ^{192}Ir active core by pure ^{169}Yb metal were calculated using Monte Carlo simulation and results were compared for the two sources in the prevalent AAPM TG-43 dosimetric formalism. Monte Carlo results were incorporated in a commercial treatment planning system and an analysis of the spectrum of inverse treatment planning solutions for prostate HDR brachytherapy in actual patient cases was performed. Findings indicate that prostate treatment with the ^{169}Yb source provides better dose homogeneity inside the PTV with lower delivered dose maxima relative to the ^{192}Ir source. The urethra objective is strongly correlated to that of homogeneity and the ^{169}Yb source also yields better dose sparing for this organ at risk relative to the ^{192}Ir source. If the rectum is not considered in the optimization procedure, use of the ^{169}Yb source could lead to increased dosage of this organ at risk relative to the ^{192}Ir source while comparable dose sparing of the bladder is achieved with both the ^{192}Ir and ^{169}Yb sources. Overall, planning quality indices (DVH, COIN) imply that prostate brachytherapy using the ^{169}Yb source is at least equivalent to the current practice of ^{192}Ir HDR prostate brachytherapy in comparable treatment times for sources of equal air kerma strength, irrespective of the prostate volume. Thus, prostate HDR brachytherapy would greatly benefit from the reduction in shielding requirements for ^{169}Yb that would preclude the need for dedicated, heavily shielded suites and patient transfer from the urology or radiology department. The production of an ^{169}Yb HDR source requires adequate levels of specific activity (90–140 GBq mg^{-1} for a source of 1.2–2.0 mm^3 active core) which necessitates high enrichment in ^{168}Yb, activation in very high neutron flux reactors, and prolonged activation times (of the order of two weeks). The currently feasible enrichment at levels as high as 85% in ^{168}Yb reduces significantly the required cooling period for the decay of ^{175}Yb contamination, which is a β^- decaying radionuclide with a 4.185 days half-life and 252 keV mean photon energy produced by the activation of the naturally occurring ^{174}Yb (31.83% natural abundance). Another challenge for the manufacture of an ^{169}Yb afterloader lies in handling the cost, safety, and time effectiveness issues arising by the need for frequent source replacement due to the short half-life of ^{169}Yb (32.012 days relative to 73.83 days for ^{192}Ir).

[a]Electronic mail: glymper@phys.uoa.gr
[b]Corresponding author. Electronic mail: dimos.baltas@klinikum-offenbach.de

[1] D. L. D. Mason, J. J. Battista, R. B. Barnett, and A. T. Porter, "Ytterbium-169: Calculated physical properties of a new radiation source for brachytherapy," Med. Phys. **19**, 695–703 (1992).
[2] M. S. MacPherson and J. J. Battista, "Dose distributions and dose rate constants for new ytterbium-169 brachytherapy seeds," Med. Phys. **22**, 89–96 (1995).
[3] A. Piermattei., L. Azario, G. Rosis, A. Soriani, G. Arcovito, R. Ragona, M Gelelli, and G. Taccini, "Dosimetry of ^{169}Yb seed model X1267," Phys. Med. Biol. **40**, 1317–1330 (1995).
[4] H. Perera, J. F. Williamson, Z. Li, V. Mishra, and A. S. Meigooni, "Dosimetric characteristics, air-kerma strength calibration and verification of Monte Carlo simulation for a new ytterbium-169 brachytherapy source," Int. J. Radiat. Oncol., Biol., Phys. **28**, 953–970 (1994).
[5] P. K. Das, V. Mishra, H. Perera, A. S. Meigooni, and J. F. Williamson, "A secondary air kerma strength standard for Yb-169 interstitial brachytherapy sources," Phys. Med. Biol. **40**, 741–756 (1995).
[6] B. Fisher, A. Porter, R. Barnett, D. Mason, E. Papiez, and J. Battista, "First clinical application of a new brachytherapy source—Ytterbium-169," Endocur. Hypertherm. Oncol. **9**, 195–199 (1993).
[7] S. M. Loft, I. P. Coles, and R. G. Dale, "The potential of ytterbium 169 in brachytherapy: a brief physical and radiobiological assessment," Br. J. Radiol. **65**, 252–257 (1992).
[8] M. M. Bé, E. Schönfeld, and J. Morel, "Evaluation of ^{169}Yb data," Int. J. Appl. Radiat. Isot. **56**, 181–188 (2002).
[9] I. Spahn, S. Takács, Yu. N. Shubin, F. Tárkányi, H. H. Coenen, and S. M. Qaim, "Cross-section measurement of the ^{169}Tm(p,n) reaction for the production of the therapeutic radionuclide ^{169}Yb and comparison with its reactor-based generation," Int. J. Appl. Radiat. Isot. **63**, 235–239 (2005).
[10] N. S. Patel, P. Fan, S. T. Chiu-Tsao, K. Ravi, W. Sherman, H. Quon, J. Pisch, H. S. Tsao, and L. B. Harrison, "Ytterbium-169: A promising new radionuclide for intravascular brachytherapy," Cardiovasc. Radiat. Med. **2**, 173–180 (2001).
[11] G. Kovács, R. Pötter, T. Loch, J. Hammer, I. K. Kolkman-Deurloo, J. J. M. C. H. de la Rosette, H. Bertermann, "GEC/ESTRO-EAU recommendations on temporary brachytherapy using stepping sources for localised prostate cancer," Radiother. Oncol. **74**, 137–148 (2005).
[12] D. J. Demanes, R. R. Rodriguez, L. Schour, D. Brandt, and G. Altieri, "High-Dose-Rate Intensity-Modulated Brachytherapy with external beam radiotherapy for prostate cancer: California endocurietherapy's 10-year results," Int. J. Radiat. Oncol., Biol., Phys. **61**, 1306–1316 (2005).
[13] R. M. Galalae *et al.*, "Long-term outcome by risk factors using conformal high-dose-rate brachytherapy (HDR-BT) boost with or without neoadjuvant androgen suppression for localized prostate cancer," Int. J. Radiat. Oncol., Biol., Phys. **58**, 1048–1055 (2004).

[14]A. Martinez, R. Galalae, G. J. Razvan, C. Mitchell, G. Gustafson, and G. Kovacs, "No apparent benefit at 5 years from a course of neoadjuvant/concurrent androgen deprivation for patients with prostate cancer treated with a high total radiation dose," J. Urol. (Paris), **170**, 2296–2301 (2003).
[15]A. C. A. Pellizzon, W. Nadalin, J. V. Salvajoli, R. C. Fogaroli, P. E. Novaes, M. A. C. Maia, and R. Ferrigno, "Results of high dose rate afterloading brachytherapy boost to conventional external beam radiation therapy for initial and locally advanced prostate cancer," Radiother. Oncol. **66**, 167–172 (2003).
[16]T. Martin, S. Roeddiger, R. Kureka, T. Dannenberg, O. Eckart, C. Kolotas, R. Heyd, B. Rogge, D. Baltas, U. Tunn, and N. Zamboglou, "3D conformal HDR brachytherapy and external beam irradiation combined with temporary androgen deprivation in the treatment of localized prostate cancer," Radiother. Oncol. **71**, 35–41 (2004).
[17]T. Martin, C. Kolotas, T. Dannenberg, G. Strassmann, H. G. Vogt, R. Heyd, B. Rogge, D. Baltas, R. Kurek, U. Tunn, and N. Zamboglou, "New interstitial HDR brachytherapy technique for prostate cancer: CT based 3D planning after transrectal implantation," Radiother. Oncol. **52**, 257–260 (1999).
[18]T. Martin, D. Baltas, R. Kurek, S. Röddiger, M. Kontova, G. Anagnostopoulos, T. Dannenberg, T. Buhleier, and G. Skazikis, "3-D conformal HDR brachytherapy as monotherapy for localized prostate cancer. A pilot study," Strahlenther. Onkol. **180**, 225–232 (2004).
[19]Y. Yoshioka, T. Nose, K. Yoshida, R.-J. OH, Y. Yamada, E. Tanaka, H. Yamazaki, T. Inoue, and T. Inoue, "High-Dose-Rate Brachytherapy as monotherapy for localized prostate cancer: a retrospective analysis with special focus on tolerance and chronic toxicity," Int. J. Radiat. Oncol., Biol., Phys. **56**, 213–220 (2003).
[20]G. Gustafson, D. Demanes, R. Rodriguez, C. Mitchell, R. Ravanera, G. Edmundson and A. Martinez, "HDR monotherapy for early stage prostate cancer: Toxicity results utilizing the Common Toxicity Criteria," Int. J. Radiat. Oncol., Biol., Phys. **57**, Suppl, Ab. 176, 230–231 (2003).
[21]R. R. Rodriguez, D. J. Demanes, G. Altieri, California Endocurietherapy Cancer Centers HDR monotherapy program for prostate cancer: Early results. Abstract and Slide Compendium of the 11th International Brachytherapy Meeting, Santa Fe (2002).
[22]A. A. Martinez, I. Pataki, G. Edmundson, E. Sebastian, D. Brabbins, and G. Gustafson, "Phase II prospective study of the use of conformal high-dose-rate brachytherapy as monotherapy for the treatment of favourable stage prostate cancer: a feasibility report," Int. J. Radiat. Oncol., Biol., Phys. **49**, 61–69 (2001).
[23]G. M. Daskalov, E. Loeffler, and J. F. Williamson, "Monte Carlo-aided dosimetry of a new high dose-rate brachytherapy source," Med. Phys. **25**, 2200–2208 (1998).
[24]D. Baltas, C. Kolotas, K. Geramani, R. Mould, G. Ioannidis, M. Kekchidi, and N. Zamboglou, "A conformal Index (COIN) to evaluate implant quality and dose specification in brachytherapy," Int. J. Radiat. Oncol., Biol., Phys., **40**, 515–524 (1988).
[25]N. Milickovic, M. Lahanas, M. Papagiannopoulou, N. Zamboglou and D. Baltas, "Multiobjective anatomy-based dose optimization for HDR-brachytherapy with constraint free deterministic algorithms," Phys. Med. Biol. **47**, 2263–80 (2002).
[26]J. F. Briesmeister (ed), "MCNP^{TM}—A General Monte Carlo *N*-Particle Transport Code: Version 4C," Report LA-13709-M, Los Alamos, NM: Los Alamos National Laboratory, 2000.
[27]Nuclear Data Database (NUDAT). Available online by the Nuclear Energy Agency (NEA) at http://db.nea.fr
[28]R. Nath, L. L. Anderson, G. Luxton, K. A. Weaver, J. F. Williamson, and A. S. Meigooni, "Dosimetry of interstitial brachytherapy sources: Recommendations of the AAPM Radiation Therapy Committee Task Group 43," Med. Phys. **22**, 209–234 (1995).
[29]M. J. Rivard, B. M. Coursey, L. A. DeWerd, W. F. Hanson, M. S. Huq, G. S. Ibbott, M. G. Mitch, R. Nath, and J. F. Williamson, "Update of AAPM Task Group No. 43 Report: A revised AAPM protocol for brachytherapy dose calculations," Med. Phys. **31**, 633–674 (2004).
[30]A. Angelopoulos, P. Baras, L. Sakelliou, P. Karaiskos, and P. Sandilos, "Monte Carlo dosimetry of a new 192Ir high dose rate brachytherapy source," Med. Phys. **27**, 2521–2527 (2000).
[31]M. Lahanas, D. Baltas, and N. Zamboglou, "A hybrid evolutionary multiobjective algorithm for anatomy based dose optimization algorithm in HDR brachytherapy," Phys. Med. Biol. **48**, 399–415 (2003).
[32]M. Lahanas, D. Baltas, S. Giannouli, and N. Zamboglou, "Global convergence analysis of fast multiobjective gradient based dose optimization algorithms for high dose rate brachytherapy," Phys. Med. Biol. **48**, 599–617 (2003).
[33]N. Milickovic, M. Lahanas, D. Baltas, and N. Zamboglou, "Comparison of evolutionary and deterministic multiobjective algorithms for dose optimization in brachytherapy," in *Proceedings of the 1st International Conference, EMO 2001, Zurich, Switzerland, Lecture Notes in Computer Science*, edited by E. Zitzler, K. Deb, L. Thiele, C. A. Coello Coello, and D. Corne, (Springer-Verlag, Berlin, 2001, Vol. 1993, pp. 167–180.
[34]M. Lahanas, D. Baltas, and N. Zamboglou, "Anatomy-based three dimensional dose optimization in brachytherapy using multiobjective genetic algorithms," Med. Phys. **26**, 1904–1918 (1999).
[35]J. Borg and D. W. O. Rogers, "Spectra and air-kerma strength for encapsulated ^{192}Ir sources," Med. Phys. **26**, 2441–2444 (1999).
[36]L. L. Anderson, "A "natural" volume-dose histogram for brachytherapy," Med. Phys. **13** 898–903 (1986).
[37]L. L. Anderson, "Dose specification and quantification of implant quality," in *Brachytherapy Physics* edited by J. F. Williamson, B. R. Thomadsen, and R. Nath (American Medical Physics, Madison, WI, 1995) pp. 343–360.